J Therm Spray Tech
https://doi.org/10.1007/s11666-024-01902-4

ORIGINAL RESEARCH ARTICLE

Tuning the Microstructure and Mechanical Properties of Al-Co-Cr-Fe-Ni-Ti Compositionally Complex Alloys Manufactured by Means of L-DED

L. Gerdt[1] · A. Hilhorst[3] · M. Müller[1] · M. Heidowitzsch[1] · J. Kaspar[1] · E. Lopez[1] · M. Zimmermann[1,2] · P. J. Jacques[3]

Submitted: 20 June 2024 / in revised form: 21 October 2024 / Accepted: 21 November 2024

Abstract In the current study, a combinatorial high-throughput screening approach based on CALPHAD simulations and experimental validation has been utilized to explore a $Co_2CrFeNi_2$-Al-Ti CCA-system. This technique, introduced by Kaspar et al. (High Entropy Alloys Mater. https://doi.org/10.1007/s44210-023-00023-x), allows to perform an accelerated alloy development within a wide compositional range and automated fabrication of graded components with varying chemical composition and microstructure. Extended by semi-automated analytical characterization of the produced samples, this approach enables to design novel compositionally complex alloys (CCAs) with promising properties for specific requirements. In our current work, a multiphase design of $L1_2$ γ'-strengthened $Co_2CrFeNi_2$-Al-Ti CCAs partially tolerating the disordered BCC-A2 or ordered B2 phases in the alloy microstructure has been utilized. The samples with three different chemical compositions were manufactured by means of laser directed energy deposition (L-DED). By subsequent two-step heat treatment, different phase compositions and microstructures have been realized with a main objective to achieve a high volume fraction of $L1_2$ γ' precipitations. Mechanical properties of investigated alloys were characterized by means of tensile tests. Depending on chemical and phase composition of the alloys, the ultimate tensile strength varied in the range of 1060-1150 MPa. The formation of BCC-B2 phase led to decreased yield to tensile strength and showed a detrimental effect on ductility of investigated alloys.

Keywords high-temperature application · applications, rapid prototyping · applications, graded coatings · microstructures, heat treatment · processing, laser cladding · processing, mechanical properties · properties

This article is an invited paper selected from presentations at the 2024 International Thermal Spray Conference, held April 29-May 1, 2024, in Milan, Italy, and has been expanded from the original presentation. The issue was organized by Giovanni Bolelli, University of Modena and Reggio Emilia (Lead Editor); Fardad Azarmi, North Dakota State University; Sara Bagherifard, Politecnico di Milano; Partha Pratim Bandyopadhyay, Indian Institute of Technology, Kharagpur; Šárka Houdková, University of West Bohemia; Heli Koivuluoto, Tampere University; Yuk-Chiu Lau, General Electric Power (Retired); Hua Li, Ningbo Institute of Materials Technology and Engineering, CAS; Sinan Müftü, Northeastern University; and Filofteia-Laura Toma, Fraunhofer Institute for Material and Beam Technology.

✉ L. Gerdt
leonid.gerdt@iws.fraunhofer.de

[1] Fraunhofer Institute for Material and Beam Technology IWS, Dresden, Germany

[2] Technische Universität Dresden, Institute of Materials Science, Dresden, Germany

[3] UCLouvain, Institute of Mechanics, Materials and Civil Engineering (iMMC), IMAP, Place Sainte Barbe 2, 1348 Louvain-la-neuve, Belgium

Introduction

High-entropy alloys (HEAs) have garnered significant interest in materials science due to their unique properties, including exceptional strength, toughness, and corrosion resistance (Ref 1, 2). In particular, high-entropy superalloys (HESAs) have emerged as a promising class of materials for high-temperature applications, such as in gas turbines and jet engines (Ref 3). A microstructure containing a ductile FCC matrix and coherent $L1_2$ precipitates often possess a good combination of strength and ductility, as well as a high wear and corrosion resistance at high temperatures (Ref 4-7). Exploration of these novel metallic

Published online: 23 December 2024

alloy systems is normally a time-consuming and cost-intensive process. Thermodynamic-based tools such as the CALPHAD method have already been used with relatively good predictive accuracy for the Al-Co-Cr-Fe-Ni-Ti senary system (Ref 7-10). Joseph et al. (Ref 7) showed that in order to avoid detrimental intermetallic phases (e.g., the sigma phase, NiAl, Ni_2AlTi and Ni_3Ti) the combined Al and Ti content should remain below 18 at.%. In a previous work (Ref 8), the effect of 0 to 12 at.% additions of Al and Ti on $Co_2CrFeNi_2$ was investigated, giving compositional boundaries to obtain an FCC (γ) matrix with $L1_2$ precipitates (γ'). However, high-throughput experimental exploration remains essential to reliably assess one system, especially when mechanical properties are considered. While this study showed that CALPHAD calculations can be used as a powerful tool for alloy pre-screening, some discrepancies between simulated and experimental data were observed, especially regarding the formation of the σ-phase. Within the experimental high-throughput screening, the mechanical properties of investigated alloys were evaluated by means of microhardness measurements. This allows to rapidly get a first idea about the material's behavior under tribological and mechanical stresses. However, the microhardness does not provide the complete information to describe the mechanical performance of metallic alloys. Therefore, in the current study, tensile tests were conducted in order to characterize the strength and ductility of selected alloys depending on chemical and phase composition. Three different compositions with microstructures comprising of (1) FCC A1 + $L1_2$, (2) FCC A1 + $L1_2$ + BCC-B2 and (3) FCC A1 + BCC-B2 have been chosen from the previous study (Ref 8):

1. $Co_2CrFeNi_2Al_{0.3}Ti_{0.3}$ (**Al5Ti5**)
2. $Co_2CrFeNi_2Al_{0.3}Ti_{0.6}$ (**Al5Ti8**)
3. $Co_2CrFeNi_2Al_{0.9}Ti_{0.4}$ (**Al11Ti5**)

One of the main aspects of the current study is to understand the impact of the BCC-B2 phase in the considered compositional field. This ordered phase is typically strong but brittle, and a large volume fraction of B2 phase is often treated as a detrimental one regarding the mechanical properties in CoCrFeNi-AlTi alloy systems (Ref 11, 12).

Materials and Methods

In order to analyze the mechanical behavior of $Co_2CrFeNi_2$-Ti_xAl_y system, cuboid specimens with a range of Al and Ti contents were fabricated by means of L-DED. Hereby, $Co_2CrFeNi_2$ (d_{10} = 45 µm, d_{90} = 90 µm (NANOVAL GmbH & Co. KG)) pre-alloyed powder as well as elemental Al and Ti powders (Al: d_{10} = 50 µm, d_{90} = 100 µm (ECKART TLS GmbH); Ti: d_{10} = 90 µm, d_{90} = 125 µm (Höganäs Germany GmbH)) were mixed to produce samples with desired chemical compositions. By modifying the rotational speed and, consequently, the feeding rates of three individual GTV PF 2/2 disk powder feeders (GTV Verschleißschutz GmbH, Germany), the chemical composition of the samples was set very close to desired nominal composition. This adjustment resulted in a modification of the composition of the respective layer. The substrate material utilized for this purpose consisted of ten-millimeter-thick plates made of stainless steel AISI 304. A precise description of the utilized technique including the mixing of different powders can be found elsewhere in (Ref 8, 13). The chemical composition of the analyzed samples is given in Table 1.

Figure 1 shows specimens with dimensions of approximately L × W × H = 55 × 10 × 2 mm^3 extracted from L-DED fabricated cuboids for tensile tests by means of wire cutting. Overall, 10 layers have been deposited to achieve the desired height of cuboids. The precise description of the deposition strategy is described in Ref 13. Prior to the cutting all samples were first heat treated at T = 1150 °C for t = 24 h in order to homogenize the microstructure and then age hardened at T = 725 °C for t = 24 h in order to stimulate the precipitation of $L1_2$ phase. After homogenization heat treatment as well as after age hardening, the specimens were water quenched. The thorough investigation of the microstructure development during this two-step heat treatment for the given compositions has been conducted by the authors in a previous study, and the description can be found in (Ref 8).

In order to conduct microstructural characterization, a JEOL JSM-7800F scanning electron microscope (SEM) equipped with an energy-dispersive spectroscopy (EDS) detector (Oxford X-Max-80, Oxford Instruments, UK) was employed. Universal testing machine (Inspect Table 50 kN, Hegewald & Peschke GmbH, Germany) was used to perform the tensile testing with a strain rate of 2 mm/min. Nanoindentation measurements were performed at room temperature using an Agilent Nano Indenter G200 equipped with a diamond Berkovich tip. The hardness and Young's modulus were calculated using the Oliver and Pharr model (Ref 14).

Results

The microstructure of the investigated samples after two-step heat treatment is depicted in Fig. 2. The chemical compositions of the samples were selected in such a manner that complex microstructures containing three different phases could be obtained after age hardening. The

Table 1 Nominal and actual compositions of the laser cladded samples measured by energy-dispersive x-ray spectroscopy (EDS) analysis

Sample	Composition	Al (at.%)	Ti (at.%)	Cr (at.%)	Fe (at.%)	Co (at.%)	Ni (at.%)
Al5Ti5	Nominal	5.0	5.0	15.3	15.3	29.6	29.7
	EDS	4.5	5.0	15.6	16.7	29.2	29.0
Al5Ti8	Nominal	5.0	8.0	14.8	14.8	26.6	28.8
	EDS	6.2	9.1	14.6	15.5	27.3	27.1
Al11Ti5	Nominal	11.0	5.0	14.3	14.3	27.6	27.7
	EDS	12.1	5.2	14.1	14.1	27.3	27.2

Fig. 1 (a) Tensile specimens extracted from L-DED fabricated cuboids by means of wire cutting, (b) dimensions of the samples.

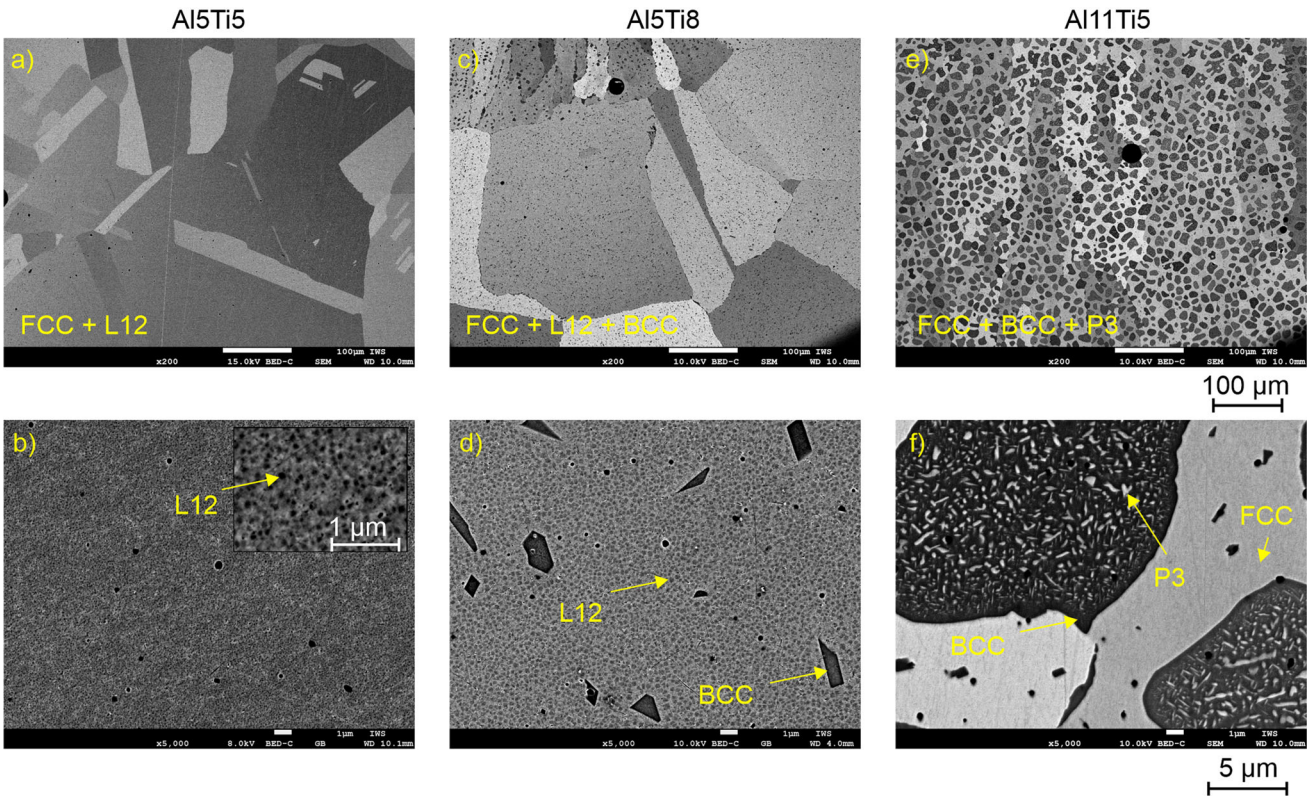

Fig. 2 SEM micrographs of the samples Al5Ti5, Al5Ti8 and Al11Ti5 after homogenization heat treatment at T = 1150 °C for t = 24°and age hardening at T = 725 °C for t = 24 h

selection is based on the results of preliminary study (Ref 8)

The microstructure of the sample with 5 at.-% Al and Ti has a dual phase microstructure consisting of FCC matrix (γ-phase) and very fine precipitations of $L1_2$ (γ'-phase), in Fig. 2(a and b). The evidence of $L1_2$ precipitation has been provided by means of SEM-EDS analysis in (Ref 8). With increased Ti amount of 8 at.-% in the sample Al5Ti8, the formation of BCC-B2 phase with a volume fraction of about 5% can be observed, in Fig. 2(c and d). After increasing Al content up to 11 at.-%, the microstructure of the samples Al11Ti5 comprises FCC A1 matrix phase, high

amount of BCC-B2 phase as well as a third phase P3 embedded inside BCC-B2 particles, in Fig. 2(e), (f). The nature of the third phase could not be clearly determined neither by means of EDS nor by EBSD analyses due to the very small particle size. Figure 3 shows the results of EBSD analysis for dual-phase microstructure of the sample Al11Ti5. The phase fraction of BCC phase calculated from this analysis amounts to 45%. The distribution of the BCC particles within the FCC matrix appears homogenous; however, many of them are located along the grain boundaries of the FCC grains, as shown in the marked area of Fig. 3(b).

The influence of the different phase compositions of the samples on their mechanical properties has been investigated by means of tensile testing. Figure 4 shows the engineering stress–strain response in uniaxial tension of the investigated alloys.

The sample Al5Ti5 exhibited the highest ductility of all series with a mean elongation-at-fracture $A = 4.6\%$. With increased content of Ti or Al and corresponding raise of the BCC-B2 phase fraction, the specimens became more brittle. The elongation-at-fracture decreased to $A = 3.9°\%$ for the composition Al5Ti8 and further to $A = 1.8\%$ for the sample Al11Ti5. A larger tensile strength is observed for specimens with complex microstructures containing FCC, BCC-B2 and P3 phases. The highest tensile strength of $R_m = 1150 \pm 30$ MPa has been measured for the sample Al11Ti5, whereas the sample Al5Ti5 exhibited a tensile strength of $R_m = 1069 \pm 60$ MPa.

The fracture surfaces of the tensile samples were subsequently analyzed by means of SEM. Figure 5 shows the micrographs of the samples after tensile tests. The sample with lower Al and Ti content exhibited a mixed fracture mode with both brittle and ductile regions. However, the brittle surfaces with trans- (TG) and intergranular (IG) features were more prevalent than ductile regions characterized by the presence of dimples, in Fig. 5d, e. The sample with increased Ti content Al5Ti8 has a significantly higher fraction of intergranular fracture. As some particles of the BCC-B2 phase could be observed at the grain boundaries of the FCC matrix, this can be considered as a possible factor for a predominant IG-failure. A typical brittle transgranular cleavage fracture could be determined for the sample with high Al content Al11Ti5, in Fig. 5c, f. For all tested specimens, the presence of small pores has been observed on the fracture surfaces. Considering the size and morphology of these pores, it can be assumed that they were formed already during manufacturing process. Therefore, these defects also affect the ductility of the analyzed specimens.

The local hardness has been measured by nanoindentation for the three different microstructures. Figure 6 shows a superposition of the hardness measurement to the corresponding SEM micrograph for each microstructure. The hardness of Al5Ti5 and Al5Ti8 both shows a homogeneous distribution with mean values of 6.9 ± 0.2 and 7.3 ± 0.1 GPa, respectively. In the case of Al11Ti5, two populations can be identified with hardness values of 5.9 ± 0.5 and 8.2 ± 0.4 GPa, respectively. The lower values are associated with the FCC matrix, while the higher values are associated with the BCC and P3 phases. The P3 phase is too fine to separate its contribution to hardness from the BCC phase. Similarly, the matrix of Al5Ti8 is harder compared to the matrix of Al5Ti5, but the contribution of the FCC matrix and the contribution of the $L1_2$ precipitate cannot be resolved.

Discussion

The behavior of single-phase FCC and $L1_2$-strengthened HEAs and CCAs under uniaxial tension condition is well studied and understood (Ref 15-17). Considerably less explored is the response of dual-phase alloys comprised of FCC and BCC phases. The results of the current study show that expected strengthening effect of hard (8.2 GPa)

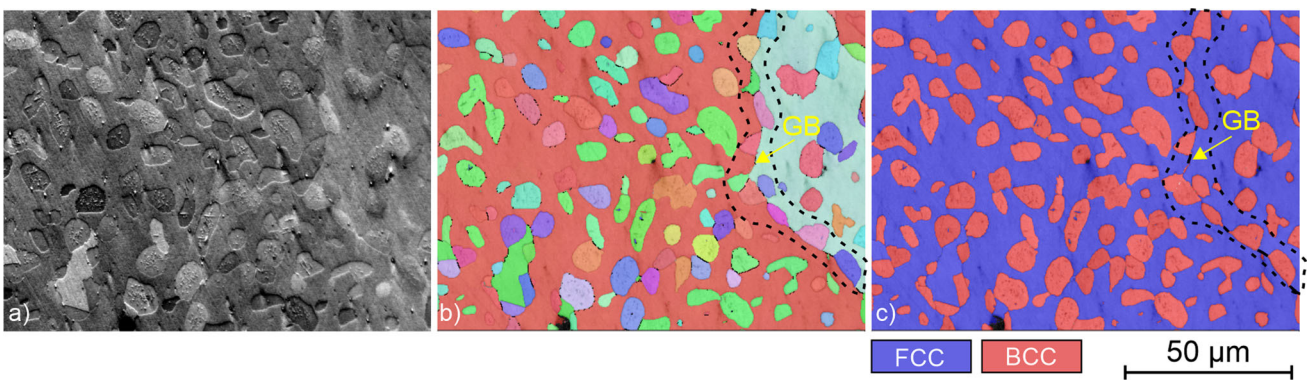

Fig. 3 (a) ForeScatter Electron (FSE) image of Al11Ti5 sample with corresponding (b) EBSD-IPF mapping and (c) EBSD-phase mapping (reuse from (Ref 8)). Grain boundary (GB) marked with yellow arrow

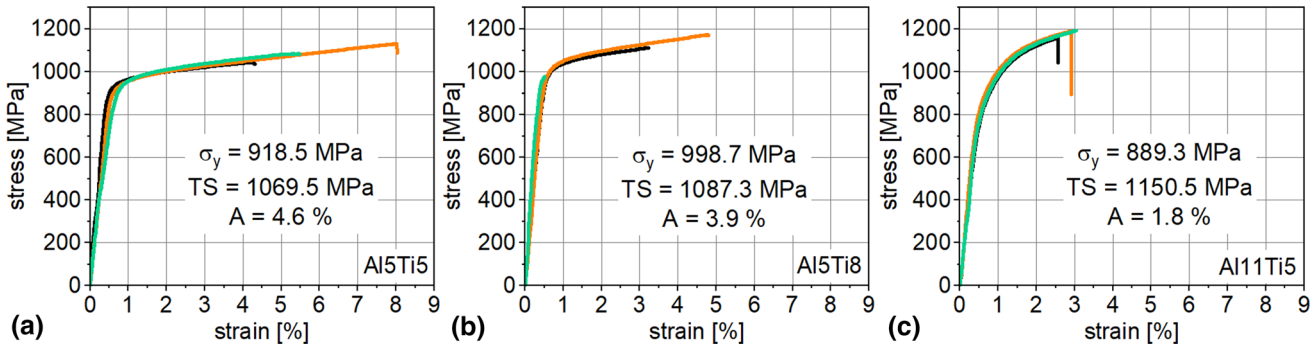

Fig. 4 Stress-strain curves of investigated alloy compositions: (a) Al5Ti5, (b) Al5Ti8 and (c) Al11Ti5 samples (colors represent three different samples each composition)

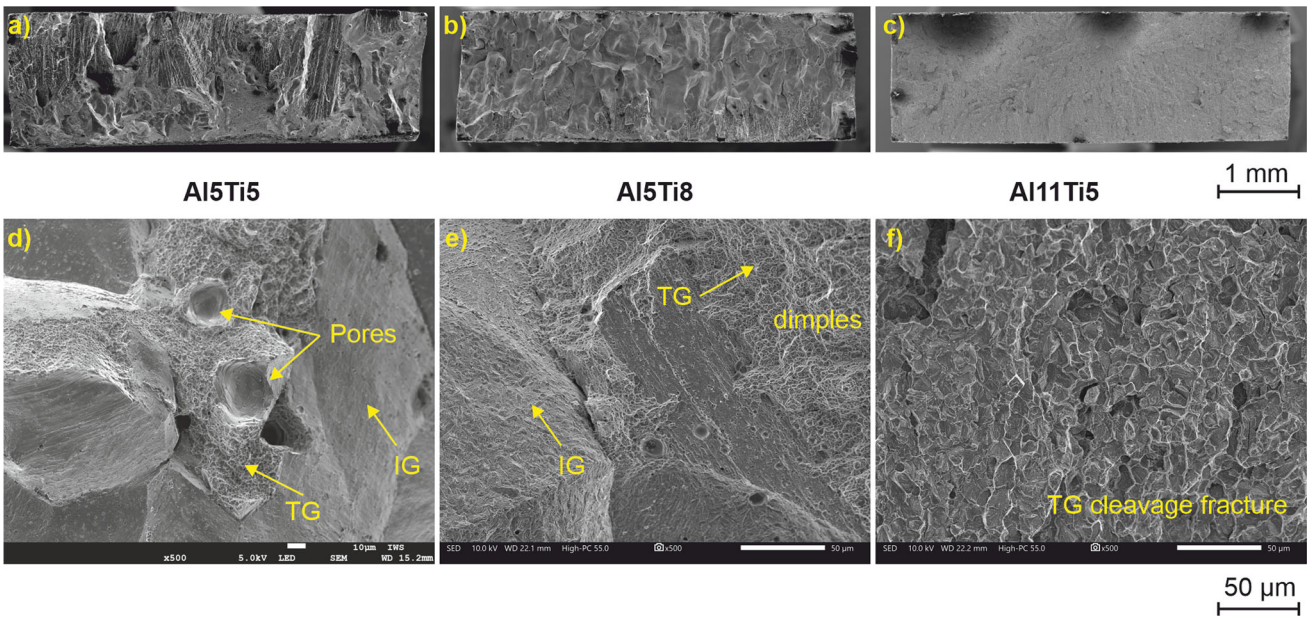

Fig. 5 SEM micrographs of fracture surfaces at different magnifications: (a) to (c) an overview of the whole fracture surface for specimens Al5Ti5, Al5Ti8 and Al11Ti5 as well as d) to f) local failure's features of these specimens, respectively

BCC phase is accompanied by a decreased ductility of the alloy Al11Ti5. These findings are in good agreement with data available from the literature (Ref 18, 19). BCC phase content in alloy Al11Ti5 accounts for 45% of the microstructure, with a mean particle size of approximately 10 µm. Even though the BCC particles are distributed quite homogenously in the sample's microstructure, they are often located at the grain boundaries of FCC grains, in Fig. 3b. This characteristic can be assumed as one of the main reasons for decreased yield strength of the dual-phase alloy Al11Ti5.

The nature of the third phase (designated as P3) embedded in BCC-B2 particles of Al11Ti5 sample could not be clarified in the course of the current study. According to the EDS analysis conducted in previous investigations (Ref 8), the formation of Ni-reach FCC and Cr- and Fe-rich BCC-A2 phases can be assumed. The structural transformation BCC-B2 → FCC as well as spinodal decomposition BCC-B2 → BCC-B2 + BCC-A2, which could lead to the observed phase transformation, was described in detail by Hecht et al. (Ref 20). Further investigation of the phase transformations in the explored alloy system during heat treatment by means of transmission electron microscopy (TEM) is the focus of a further research survey.

For the compositions Al5Ti5 and Al5Ti8, the strengthening effect of $L1_2$ precipitations in FCC matrix shown by nanoindentation experiments is also reflected in increased yield strength of the alloy with higher amount of Ti (8 at.-%). A much lower content of BCC phase in this alloy compared to Al11Ti5 seems to be less detrimental for alloy's ductility. The matrix hardness of Al11Ti5 sample is lower, compared to other compositions, due to the lack of strengthening by $L1_2$ precipitations. Moreover, a large

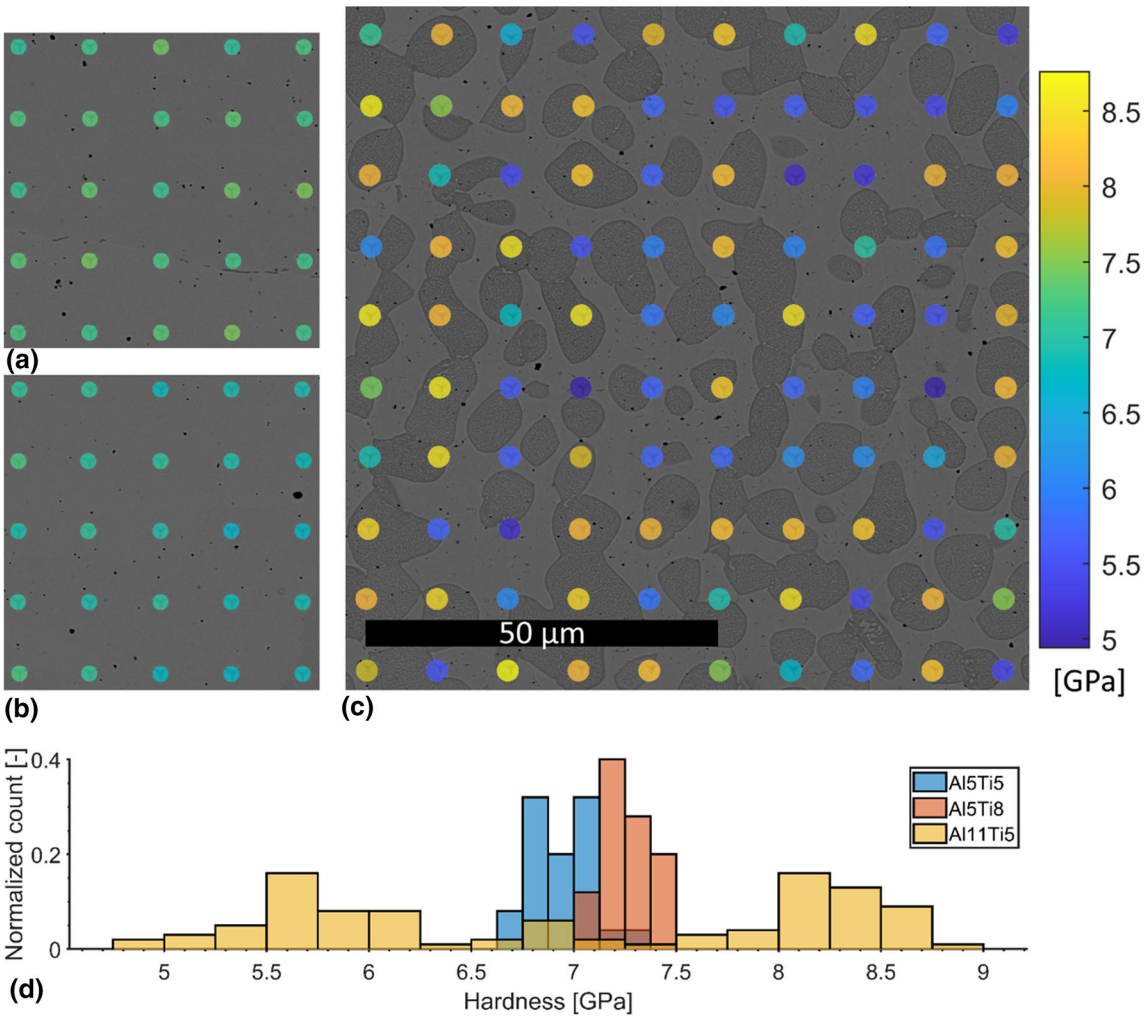

Fig. 6 Hardness measurements by nanoindentation for (a) Al5Ti5, (b) Al5Ti8 and (c) Al11Ti5 shown on top of the corresponding microstructure. The corresponding histograms are shown in (d)

variability in fracture strain is observed, indicating an early failure caused by manufacturing defects.

Conclusion

In the current work, the effect of phase composition and microstructure of three different CCAs on the basis of Co2CrFeNi2-Al-Ti CCA-system on the static mechanical properties were investigated. Besides the characterization of macroscopic behavior of the alloys during tensile testing, the properties of FCC/$L1_2$ and BCC-B2 phases have been examined by nanoindentation tests. Following conclusions can be drawn from the aforementioned findings:

1. The strengthening of the FCC phase by $L1_2$ precipitations has been confirmed both by nanoindentation and tensile tests. The higher Ti content of Al5Ti8 sample resulted in higher hardness of the FCC/$L1_2$ phase (7.3 ± 0.1 GPa) compared to the lower alloyed Al5Ti5 composition (6.9 ± 0.2 GPa). It can be explained by a higher expected amount of $L1_2$ precipitates due to the increased Ti content, as it has been predicted by CALPHAD calculations in a previous study by the authors (Ref 8).
2. High amount of the BCC-B2 phase, which is caused by extensive alloying with Al in Al11Ti5 sample, results in increased tensile strength accompanied by a significant decrease of ductility. The formation of Al- and Ni-rich BCC-B2 phase leads to depletion of Al in FCC matrix and, therefore, inhibits the strengthening by $L1_2$ precipitates.
3. The preferred localization of the BCC-B2 phases at the grain boundaries of the FCC structure may additionally affect the ductility of the alloy Al11Ti5.

Funding Open Access funding enabled and organized by Projekt DEAL. The current work was conducted within the M-ERA.NET Project "Novel metallic materials, feedstock and fabrication process for high-performance additive manufactured goods." This project is co-financed with tax funds on the basis of the budget passed by the Saxon state parliament. A.H., A.M.B. and P.J.J. acknowledge the financial support from the NovMatAM project (convention No. 2010095) funded by the Service public de Wallonie, Economie Emploi Recherche (SPWEER), as well as the help of the LACaMi technological platform of UCLouvain.

References

1. N. Yurchenko, N.D. Stepanov, S.V. Zherebtsov, M.A. Tikhonovsky and G.A. Salishchev, Structure and Mechanical Properties of B2 Ordered Refractory AlNbTiVZr x (x = 0-1.5) High-Entropy Alloys, *Mater. Sci. Eng. A*, 2017, **704**, p 82-90. https://doi.org/10.1016/j.msea.2017.08.019
2. E.P. George, W.A. Curtin and C.C. Tasan, High Entropy Alloys: A Focused Review of Mechanical Properties and Deformation Mechanisms, *Acta Mater.*, 2020, **188**, p 435-474. https://doi.org/10.1016/j.actamat.2019.12.015
3. J. Chen, X. Zhou, W. Wang, B. Liu, Y. Lv, W. Yang, D. Xu and Y. Liu, A Review on Fundamental of High Entropy Alloys with Promising High-Temperature Properties, *J. Alloys Compd.*, 2018, **760**, p 15-30. https://doi.org/10.1016/j.jallcom.2018.05.067
4. Y.-J. Chang and A.-C. Yeh, The Evolution of Microstructures and High Temperature Properties of AlxCo1.5CrFeNi1.5Tiy High Entropy Alloys, *J. Alloys Compd.*, 2015, **653**, p 379-385. https://doi.org/10.1016/j.jallcom.2015.09.042
5. H.M. Daoud, A.M. Manzoni, N. Wanderka and U. Glatzel, High-Temperature Tensile Strength of Al10Co25Cr8Fe15Ni36Ti6 Compositionally Complex Alloy (High-Entropy Alloy), *JOM*, 2015, **67**(10), p 2271-2277. https://doi.org/10.1007/s11837-015-1484-7
6. J.-X. Hou, B.-X. Cao, B. Xiao, Z.-B. Jiao and T. Yang, Compositionally Complex Coherent Precipitation-Strengthened High-Entropy Alloys: A Critical Review, *Rare Met.*, 2022, **41**(6), p 2002-2015. https://doi.org/10.1007/s12598-021-01953-4
7. J. Joseph, M. Annasamy, S.R. Kada, P.D. Hodgson, M.R. Barnett and D.M. Fabijanic, Optimising the Al and Ti Compositional Window for the Design of γ' (L12)-Strengthened Al-Co-Cr-Fe-Ni-Ti High Entropy Alloys, *Mater. Sci. Eng. A*, 2022, **835**, p 142620. https://doi.org/10.1016/j.msea.2022.142620
8. J. Kaspar, A. Hilhorst, L. Gerdt, M. Müller, M. Heidowitzsch, M. Kuczyk, A.M. Bettanini, P.J. Jacques, M. Zimmermann and C. Leyens, Combinatorial Alloy Design and Microstructure Evolution in Laser-Cladded Al-Co-Cr-Fe-Ni-Ti Compositionally Complex Alloys, *High Entropy Alloys Mater.*, 2023 https://doi.org/10.1007/s44210-023-00023-x
9. T. Rieger, J.-M. Joubert, M. Laurent-Brocq, L. Perrière, I. Guillot and J.-P. Couzinié, Study of the FCC+L12 Two-Phase Region in Complex Concentrated Alloys Based on the Al-Co-Cr-Fe-Ni-Ti System, *Materialia.*, 2020, **14**, p 100905. https://doi.org/10.1016/j.mtla.2020.100905
10. T. Rieger, J.-M. Joubert, R. Poulain, X. Sauvage, E. Paccou, L. Perrière, I. Guillot, G. Dirras, G. Laplanche, M. Laurent-Brocq and J.-P. Couzinié, Influence of Chemical Composition on Coarsening Kinetics of Coherent L12 Precipitates in FCC Complex Concentrated Alloys, *J. Alloys Compds.*, 2023, **967**, p 171711. https://doi.org/10.1016/j.jallcom.2023.171711
11. Z. Li, L. Fu, J. Peng, H. Zheng, X. Ji, Y. Sun, S. Ma and A. Shan, Improving Mechanical Properties of an FCC High-Entropy Alloy by γ′ and B2 Precipitates Strengthening, *Mater Charact*, 2020, **159**, p 109989. https://doi.org/10.1016/j.matchar.2019.109989
12. J. Joseph, N. Stanford, P. Hodgson and D.M. Fabijanic, Understanding the Mechanical Behaviour and the Large Strength/Ductility Differences Between FCC and BCC AlxCoCrFeNi High Entropy Alloys, *J. Alloys Compd.*, 2017, **726**, p 885-895. https://doi.org/10.1016/j.jallcom.2017.08.067
13. M. Müller, C.C. Labisch, L. Gerdt, L. Bach, M. Riede, J. Kaspar, E. López, F. Brueckner, M. Zimmermann and C. Leyens, Multimaterial Direct Energy Deposition: From Three-Dimensionally Graded Components to Rapid Alloy Development for Advanced Materials, *J. Laser Appl.*, 2023, **35**(1), p 12006. https://doi.org/10.2351/7.0000788
14. W.C. Oliver and G.M. Pharr, An Improved Technique for Determining Hardness and Elastic Modulus Using Load and Displacement Sensing Indentation Experiments, *J. Mater. Res.*, 1992, **7**(6), p 1564-1583. https://doi.org/10.1557/JMR.1992.1564
15. B.X. Cao, H.J. Kong, Z.Y. Ding, S.W. Wu, J.H. Luan, Z.B. Jiao, J. Lu, C.T. Liu and T. Yang, A Novel L12-Strengthened Multicomponent Co-Rich High-Entropy Alloy with Both High γ′-Solvus Temperature and Superior High-Temperature Strength, *Script. Mater.*, 2021, **199**, p 113826. https://doi.org/10.1016/j.scriptamat.2021.113826
16. B. Gludovatz and R.O. Ritchie, Fracture Properties of High-Entropy Alloys, *MRS Bull.*, 2022, **47**(2), p 176-185. https://doi.org/10.1557/s43577-022-00267-9
17. S. Gorsse, M.H. Nguyen, O.N. Senkov and D.B. Miracle, Database on the Mechanical Properties of High Entropy Alloys and Complex Concentrated Alloys, *Data Brief*, 2018, **21**, p 2664-2678. https://doi.org/10.1016/j.dib.2018.11.111
18. N. Birbilis, S. Choudhary, J.R. Scully and M.L. Taheri, A Perspective on Corrosion Of Multi-Principal Element Alloys, *NPJ Mater. Degradat.*, 2021, **5**(1), p 248. https://doi.org/10.1038/s41529-021-00163-8
19. L. Liu, Y. Zhang, Z. Zhang, Z. Wang and L. Sun, Achieving Exceptional Strength-Ductility Synergy in a Dual-Phase High Entropy Alloy Via Architected Complex Microstructures, *Mater. Sci. Eng. A*, 2023, **882**, p 145413. https://doi.org/10.1016/j.msea.2023.145413
20. U. Hecht, S. Gein, O. Stryzhyboroda, E. Eshed and S. Osovski, The BCC-FCC Phase Transformation Pathways and Crystal Orientation Relationships in Dual Phase Materials from Al-(Co)-Cr-Fe-Ni Alloys, *Front. Mater.*, 2020, **7**, p 238. https://doi.org/10.3389/fmats.2020.00287
21. T. Yang, Y. Zhao, W. Liu, J. Kai and C. Liu, L1 2-Strengthened High-Entropy Alloys for Advanced Structural Applications, *J. Mater. Res.*, 2018, **33**(19), p 2983-2997. https://doi.org/10.1557/jmr.2018.186
22. T.-K. Tsao, A.-C. Yeh, C.-M. Kuo and H. Murakami, On the Superior High Temperature Hardness of Precipitation

Strengthened High Entropy Ni-Based Alloys, *Adv. Eng. Mater.*, 2017, **19**(1), p 1600475. https://doi.org/10.1002/adem.201600475

23. D. Hausmann, C. Solís, L.P. Freund, N. Volz, A. Heinemann, M. Göken, R. Gilles and S. Neumeier, Enhancing the High-Temperature Strength of a Co-Base Superalloy by Optimizing the γ/γ' Microstructure, *Metals.*, 2020, **10**(3), p 321. https://doi.org/10.3390/met10030321